Sources of Intensity Nonuniformity in Spin Echo Images at 1.5 T

Andrew Simmons, Paul S. Tofts, Gareth J. Barker, Simon R. Arridge

This manuscript describes a number of sources of nonuniformity for spin echo images at 1.5 T. Both coil tuning and crosstalk can have significant effects on image nonuniformity. For short repetition times, nonuniformity increases with decreasing *TR*, possibly due to gradient eddy currents. In sections of RF coils with poor RF uniformity, image nonuniformity varies with both echo time and the number of echoes in a multiecho sequence. For the particular imager used, there are small differences between transverse and sagittal/coronal nonuniformity. The temporal stability of image nonuniformity is very good. The use of uniform oil phantoms is shown to be superior to low pass filtered images for correction of image nonuniformity.

Key words: MRI; magnetic resonance imaging; nonuniformity; spin echo.

INTRODUCTION

An MR image of a uniform sample may demonstrate areas of nonuniform signal intensity. Such nonuniformity is also present in patient data and may affect diagnosis. It is necessary to measure nonuniformity for comparison of the uniformity of different radio frequency (RF) coils, calculation of proton density images, and correction of nonuniformity for intensity-based segmentation methods (1, 2). Nonuniformity is therefore an important part of a quality assurance (QA) program (3). Our interest is primarily for the correction of nonuniformity prior to intensity-based segmentation.

Previously other authors and ourselves have noted several potential sources of nonuniformity (4, 5) including B_0 inhomogeneity, bandwidth filtering of data, RF transmission and reception inhomogeneity, RF standing waves, and RF penetration effects.

The use of a spin echo sequence compensates for spin dephasing caused by B_0 inhomogeneity which can therefore be ignored for standard imaging conditions. Many MR imagers utilize a time domain filter to reduce incoming data to a bandwidth below the Nyquist frequency, which can attenuate intensity near the edge of the image. If the amplitude of the RF transmission field varies across an image then under-flipping and over-flipping of spins occurs, both of which produce a reduction in signal intensity. Receive coil nonuniformity can produce both increases and decreases in signal intensity and uniformity is often sacrificed somewhat for the sake of signal to noise ratio (SNR). For the GE Signa used for these studies (General Electric, Milwaukee, WI), the same circularly polarized birdcage head or body coil is usually used for both transmission and reception; the use of separate coils (e.g., phased array or other surface coils) for transmission and reception is not considered here.

RF standing waves occur in cylindrical phantoms at 1.5 T with a wavelength dependent upon the permittivity of the sample (6). The wavelength for a circularly polarized coil, λ, is

$$\lambda = \frac{2\pi}{\omega\left(\frac{1}{2}\epsilon_r\epsilon_0\mu_r\mu_0\left(\left[1+\frac{1}{\rho^2\epsilon_r^2\epsilon_0^2\omega^2}\right]^{1/2}+1\right)\right)^{1/2}} \quad [1]$$

(ω = frequency of magnetic field, ϵ_r = relative permittivity, ϵ_0 = permittivity of free space, μ_r = relative permeability, μ_0 = permeability of free space, ρ = resistivity of medium). At 1.5 T λ(water) = 0.52 m and λ(oil) = 2.09 m [ϵ_r(water) = 80, ϵ_r(oil) = 5, μ_r(water) = μ_r(oil) = 1 (7)]. Some authors (8, 9) have failed to distinguish this effect from other sources of nonuniformity when using water phantoms at 1.5 T.

The conductivity of a sample may lead to an RF skin depth or penetration effect, giving a sample dependent RF field distortion. The skin depth (10), δ, is given by

$$\delta = \sqrt{2/\mu_r\mu_0\omega\sigma} \quad [2]$$

where σ is the sample's conductivity. The skin depth of physiological saline ($\sigma = 1.00(\Omega m)^{-1}$) is 6.3 cm, while the skin depth of oil is effectively infinite. Effects in biological tissue are likely to be less than those predicted by models based on uniform conduction medium (e.g., (11)) because there are insulating structures that prevent large diameter current loops from forming.

Both RF penetration effects and RF standing waves are negligible for oil phantoms and the human head at 1.5 T (6). A large cylindrical oil phantom of diameter 27.7 cm with its axis oriented parallel to the magnet axis has therefore been used where necessary throughout this work.

Various approaches to image nonuniformity correction have been reported in the literature. Condon *et al.* (4) corrected for RF receiver nonuniformity and bandwidth filtering of head images at 0.15 T using water phantom images and a mathematical fit to the form of the filter. Wicks *et al.* corrected patient images of any orientation at 0.5 T for RF receiver nonuniformity using three orthogonal datasets of a uniform phantom (5). Other authors (12,

MRM 32:121–128 (1994)

From the Departments of Medical Physics (A.S.), and Computer Science (S.R.A.), UCL; and NMR Research Group, Institute of Neurology (A.S., P.S.T., G.J.B.), London, United Kingdom.

Address correspondence to: Andrew Simmons, Ph.D., Nuclear Medicine Department, Kent and Canterbury Hospital, Ethelbert Road, Canterbury, Kent CT1 3NG, United Kingdom.

Received November 17, 1993; revised March 14, 1994; accepted March 14, 1994.

This work was supported by the British Science and Engineering Research Council and Picker UK (to A.S.). The MRI imager was generously funded by the Multiple Sclerosis Society of Great Britain and Northern Ireland.

0740-3194/94 $3.00

13) have used similar methods to correct surface coil images of the spine. McVeigh *et al.* (14) and Nelson *et al.* (15) calculated RF coil inhomogeneity using numerical integration of the Biot Savart law to enable correction. Several authors have used low pass filtering of patient images to estimate nonuniformity (16–20).

We describe a number of important additional sources of spin echo intensity nonuniformity, discuss the temporal stability of image nonuniformity and compare nonuniformity correction with oil filled phantoms to a typical low pass filtering based method. Although measurements are presented for a specific imager (a 1.5 T GE Signa Advantage imager with actively shielded gradients running 4.7 software), the methods are applicable to all machines, and the results give an indication of what may be expected for other modern 1.5 T machines.

METHOD

Nonuniformity of the Geometry of Image Planes

The size and shape of image planes are affected by slice warp and in-slice geometric distortions that lead to a variation in voxel volume with position and produce corresponding signal intensity nonuniformities. It is important to quantify these sample independent effects before considering other sources of nonuniformity. Measurements of slice warp, the distortion of a slice along the slice select direction, have been made using the Eurospin II test object 3 (21). Sample independent geometric distortions due to B_0 nonuniformity and gradient nonlinearities have been measured using a circular solid perspex phantom with an array of holes each filled with doped water.

Bandwidth Filtering of the Data

As discussed in the Introduction, bandwidth filtering of data can affect image uniformity (4, 5). Sagittal, coronal, and axial images of air were acquired in order to provide an indication of the effect of bandwidth filtering on image noise.

Mistuning of the Head Coil

The RF coil is assumed to have uniform response across the range of Larmor frequencies used, both for slice selection during transmission, and for frequency encoding with a read gradient during reception. With the advent of higher gradients, both for slice selection (to allow thinner slices), and for read out (to allow high bandwidths and echo planar sequences), these assumptions must be reexamined.

The RF field B_1 produced by a coil varies with resonant frequency (22) as

$$B_1 = \frac{B_{10}}{[1 + 4Q^2(f_L/f_0 - 1)^2]^{1/2}} \quad [3]$$

(f_L = Larmor frequency, f_0 = resonant frequency of coil, Q = quality factor of coil, B_{10} = RF field strength with coil on resonance). If the coil is resonated close to the centre of its range of resonance frequencies the fractional change in B_1 values across the image can be shown by Taylor expansion of equation (3) in terms of $(f_L/f_0 - 1)$ to be

$$\left(\frac{\Delta B_1}{B_{10}}\right)_{\text{near resonance}} = \frac{1}{2}\left(\frac{Q \cdot BW}{f_0}\right)^2 \quad [4]$$

where BW is the image bandwidth or range of Larmor frequencies and $f_L = f_0 \pm BW/2$.

If the coil is off-tune then the variation of B_1 with Larmor frequency is increased, and asymmetrical. Over a small range of frequencies the fractional change in B_1 values across the image with the coil tuned to one of the 3 *dB* points of its resonance curve can be shown by differentiation to be

$$\left(\frac{\Delta B_1}{B_{10}}\right)_{3dB} = \frac{Q \cdot BW}{\sqrt{2} f_0} \quad [5]$$

During transmission the range of excitation frequencies present for slice selection with a gradient strength G is $BW = \gamma \cdot G \cdot \text{FOV}_{\text{slice}}$ where $\text{FOV}_{\text{slice}}$ is the field of view in the slice direction. For a 10 mT/m slice selection gradient, and 20 cm $\text{FOV}_{\text{slice}}$, BW = 85 kHz. Assuming Q = 100 at 1.5 T (64 MHz), the spread of B_1 values with the coil on tune (Eq. [4]) is 1%, and with the coil off-tune at the 3 *dB* point is 10% (Eq. [5]). During reception, conventional bandwidths are typically 32 kHz, in which case the range of B_1 values is 0.1% on tune, and 4% at the 3 *dB* point. Fast gradient echo and echo planar pulse sequences use much higher bandwidths, however. At 250 kHz the range of B_1 values on tune is 8%, and at the 3 *dB* point off tune is 28%.

On some NMR systems the coil can be tuned for each object. The Signa head coil, a high pass birdcage coil, is tuned to approximately 250 kHz above the Larmor frequency of 64 MHz (Personal communication - M. Suminski, GE, Waukesha, WI). The presence of a patient's head within the coil leads to stray capacitance between the end ring and the patient's shoulders causing a drop in resonant frequency of the coil to approximately 64 MHz. This frequency shift may be achieved during phantom studies by the use of a "tuning ring" comprising small patches of copper on a plastic former (23). The variation in nonuniformity due to mistuning has been investigated by imaging a hexagonal packed array of water bottles both with and without the tuning ring.

The Effect of Crosstalk on Contiguous Slice Datasets

A variation of intensity with slice position has been reported to occur in an alternating stepping manner, being due to either gradient eddy currents (5, 24) or, more convincingly, to crosstalk between slices (25). We show that this stepping only occurs for even numbers of slices. Crosstalk can occur even for interleaved slice acquisition (i.e., where first data is collected from even numbered slices, and then from odd numbered slices). This stepping may be explained by considering a simple model of a 10-slice contiguous data acquisition with slices acquired in an interleaved manner at intervals of 100 ms, for a total *TR* of 1000 ms (i.e., slice 1 at 0 ms, slice 2 at 500 ms, slice 3 at 100 ms, etc.) (Fig. 1, after (25)). Crosstalk leads to adjacent slices being partially excited in addition

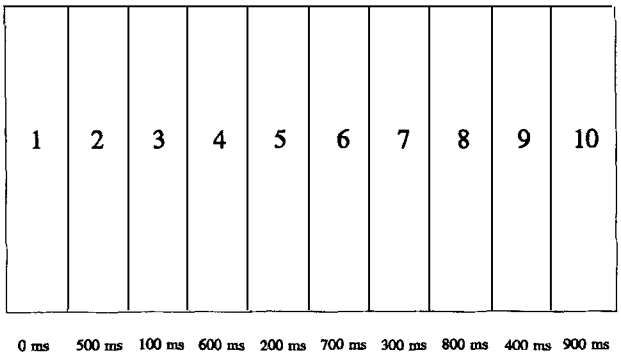

FIG. 1. Model of 10 slice contiguous data acquisition with slices acquired in an interleaved manner (i.e., in the order 1,3,5,7,9,2,4,6,8,10). Each slice is excited at intervals of 100 ms (*TR* = 1000 ms).

to the slice of interest. Thus, for example, excitation of slice 6 also partially excites some spins in slices 5 and 7. With even numbers of slices in a contiguous block, even and odd numbered slices have different times in which to relax after being partially excited by neighboring slice RF pulses. As an example, consider slice 6 at the time of its slice acquisition. The last time that it was partially excited, by acquisition of slice 7, was 400 ms ago, and by acquisition of slice 5, 500 ms ago. This can be contrasted with slice 5, which was partially excited by the acquisition of slice 6, 500 ms ago and by the acquisition of slice 4, 600 ms ago (both in the previous *TR* period). By a similar argument, it can be shown that there will be no such effect for datasets with an odd number of slices. The variation in crosstalk with number of slices has been studied by acquiring contiguous slice datasets of 3, 4, 5, 6, 7, and 8 slices of a large oil phantom using a SE 300/20 pulse sequence with 5-mm thick slices.

Variation of Nonuniformity with *TR*

It has been postulated that uncompensated gradient eddy-currents present during selective pulses may select a slice of different thickness or position to that required, or cause de-phasing resulting in signal loss (5, 24). In order to investigate the magnitude of any gradient eddy-current effects, single slice images were acquired in the head coil with a range of *TR*s (*TE* = 40 ms, *TR* = 60–3000 ms). Ratio images, the result of dividing one image by another, were used to compare nonuniformity at different *TR*s. In order to isolate RF transmit and receive nonuniformity effects from any gradient eddy-current effects, a second set of images were acquired in the body coil using the same parameters. The body coil provides more uniform RF transmission and reception at the expense of poorer SNR. Further images of multislice datasets were acquired at long *TR*s, to investigate whether multislice acquisition, which puts more load on the gradient power supply and coils than single slice acquisition, might induce gradient eddy-currents for long *TR*s.

Variation of Nonuniformity with *TE*

The possibility of variation of nonuniformity with *TE* was investigated at a long *TR* (3000 ms) with a single echo pulse sequence for a range of *TE*s (20–160 ms) in both the head coil and the body coil.

Variation of Nonuniformity with Number of Echoes

In order to investigate any variation of nonuniformity with the number of echoes per sequence, a range of four echo datasets was acquired with a given echo time varying in position in the echo train between datasets. For example, a 40-ms echo might be acquired as the first echo in a 40/80/120/160-ms echo train, or second echo in a 20/40/60/80-ms echo train. This allows comparison of the effect of position within the echo train without variation of echo time biasing results.

Difference Between Transverse and Sagittal or Coronal Images

Prompted by earlier investigations, data was acquired at the maximum recommended distance superior to the head coil center in transverse, sagittal, and coronal orientations. The image intensity at a range of points was compared between the three orientations, both with and without the use of a GE proprietary algorithm (GRADWARP) for correction of gradient nonlinearity-based geometric distortions.

Temporal Stability of Nonuniformity Measurements

It is important that image nonuniformity is stable with time in order that regular measurements are not necessary for nonuniformity correction based on images of uniform phantoms. A large oil phantom was imaged monthly for 6 months using a set protocol (SE 3000/80). Each dataset was median filtered to reduce noise and comparisons were made using ratio images of the first dataset with each subsequent dataset.

Correction of RF Nonuniformity

There are several methods of correcting for image nonuniformity, as discussed in the Introduction. The use of Biot Savart law simulations has been discounted as this does not take into account manufacturing imperfections and other potential sources of nonuniformity. A typical low pass filtering-based technique (that of Lim and Pfefferbaum (20)) has been implemented that consists of automatically isolating the brain and "feathering" the isolated brain by taking the average gray level on radii emanating from the center of gravity of the image and replicating this value from the edge of the brain to the edge of the image. The resulting image is low pass filtered using a 33 × 33 averaging filter and smoothed using a 3 × 3 gaussian filter. The final image is claimed to represent image nonuniformity and has been compared with an image of a uniform phantom acquired in the same position and orientation.

RESULTS

Nonuniformity of the Geometry of Image Planes

Measurements of sample independent geometric distortions indicate no significant slice warp or sample independent geometric distortions for the imager used for this

work (26). It should be noted that image reconstruction on the Signa includes a proprietary algorithm for gradient nonlinearity correction, which is discussed in more detail below under "Difference Between Transverse and Sagittal or Coronal Images." Sample dependent geometric distortions due to local susceptibility differences and the chemical shift effect can cause significant distortions in biological samples, however (26).

Bandwidth Filtering of the Data

Visual and quantitative region of interest analysis of noise mean and standard deviation showed no variation with position within the images except for the edge 2 or 3 pixels in the frequency encoding direction. The Signa utilizes a high frequency analogue filter prior to digitizing the signal to avoid aliasing; the signal is then oversampled by at least a factor of 4 and a digital filter used to define the final bandwidth. The effect of the Signa's digital filter may therefore be ignored. Condon *et al.* (4) have discussed methods for the correction of more severe effects.

Mistuning of the Head Coil

Figure 2 illustrates images acquired (a) with, and (b) without the tuning ring. Both images have been thresholded to the same level; image (a) shows clear asymmetry while image (b) shows the approximately circular symmetry expected from the coil design (27). The magnitude of asymmetry of the former image leads to a maximum difference of approximately 9% in signal between bottles at opposite sides of the image. This compares with less than a 1% difference for the latter case. The tuning ring was therefore used for all phantom work.

The Effect of Crosstalk on Contiguous Slice Datasets

Figure 3 illustrates the variation in mean intensity of a small region at the center of the field of view with slice number for various contiguous slice datasets of 3 to 8 slices. The distinct stepping is clear for an even number of slices and contrasts with the small difference for odd numbers of slices. The intensity of the end slices is higher than other slices; this is to be expected as end slices experience less partial saturation. Crosstalk can be avoided or substantially reduced by either noncontiguous acquisition techniques (25) or better shaped RF pulses (28).

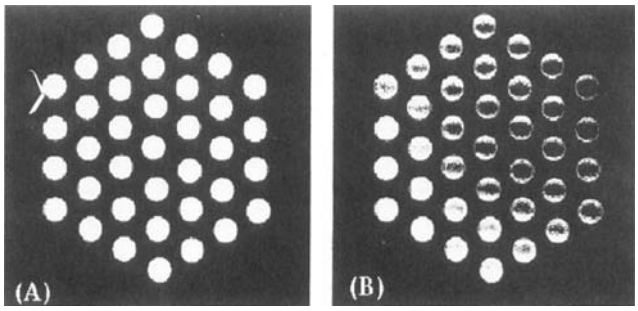

FIG. 2. Array of bottles filled with manganese chloride solution and imaged in an axial plane in the head coil (a) with, and (b) without the manufacturer's tuning ring. The nonuniformity of (b) is a result of mistuning of the head coil.

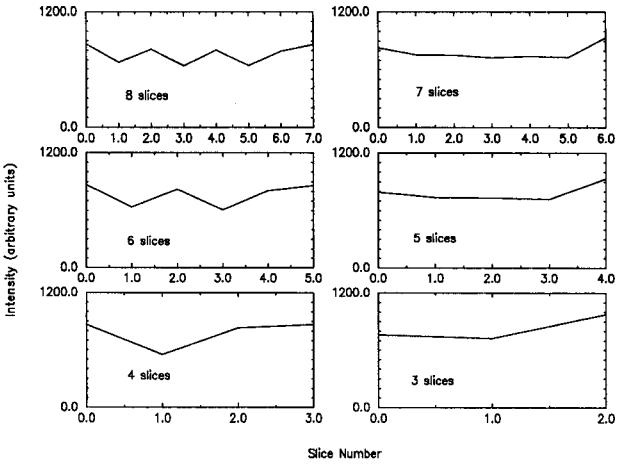

FIG. 3. Variation of crosstalk in superior/inferior direction with number of slices for standard slice profile contiguous slice axial datasets acquired using the head coil.

Variation of Nonuniformity with *TR*

For long *TR*s (greater than 1000 ms), there were no variations in nonuniformity between images acquired using the head coil. Figure 4a illustrates a profile through a ratio image of a SE 3000/40 image divided by a SE 1000/40 image, which is virtually uniform (apart from the Gibbs artifact at the phantom edges). Comparison of long *TR* images with progressively shorter *TR* images, however, demonstrated increasing differences between the nonuniformity of the images, with small variations first apparent at a *TR* of 500 ms. Figure 4b, a profile through a ratio image of a SE 3000/40 image divided by a SE 60/40 image, demonstrates distinct nonuniformity with a sharp drop off toward both sides of the phantom. Figure 4c illustrates that for long repetition times, uniformity is also virtually constant for the body coil. The major distortions apparent for shorter *TR*s were still apparent with the body coil images as demonstrated by Figure 4d. These results suggest the presence of gradient eddy-current effects with a short characteristic time constant. Figure 4e illustrates a profile through the ratio image of a single slice image divided by the equivalent from a multislice image. The ratio image is uniform, demonstrating the absence of any additional gradient eddy-currents due to multislice acquisition. Thus, although the variation of nonuniformity with repetition time is suggestive of gradient eddy-currents, the apparent absence of eddy-currents from multislice images is a discrepancy for which we have no explanation.

Variation of Nonuniformity with *TE*

Figure 5a illustrates profiles through a SE 3000/20 image divided by both a SE 3000/40 and SE 3000/80 image for the head coil. Dividing late echo images by early echo images demonstrates drop off of the ratio image in the poor homogeneity sections of the head coil. For small

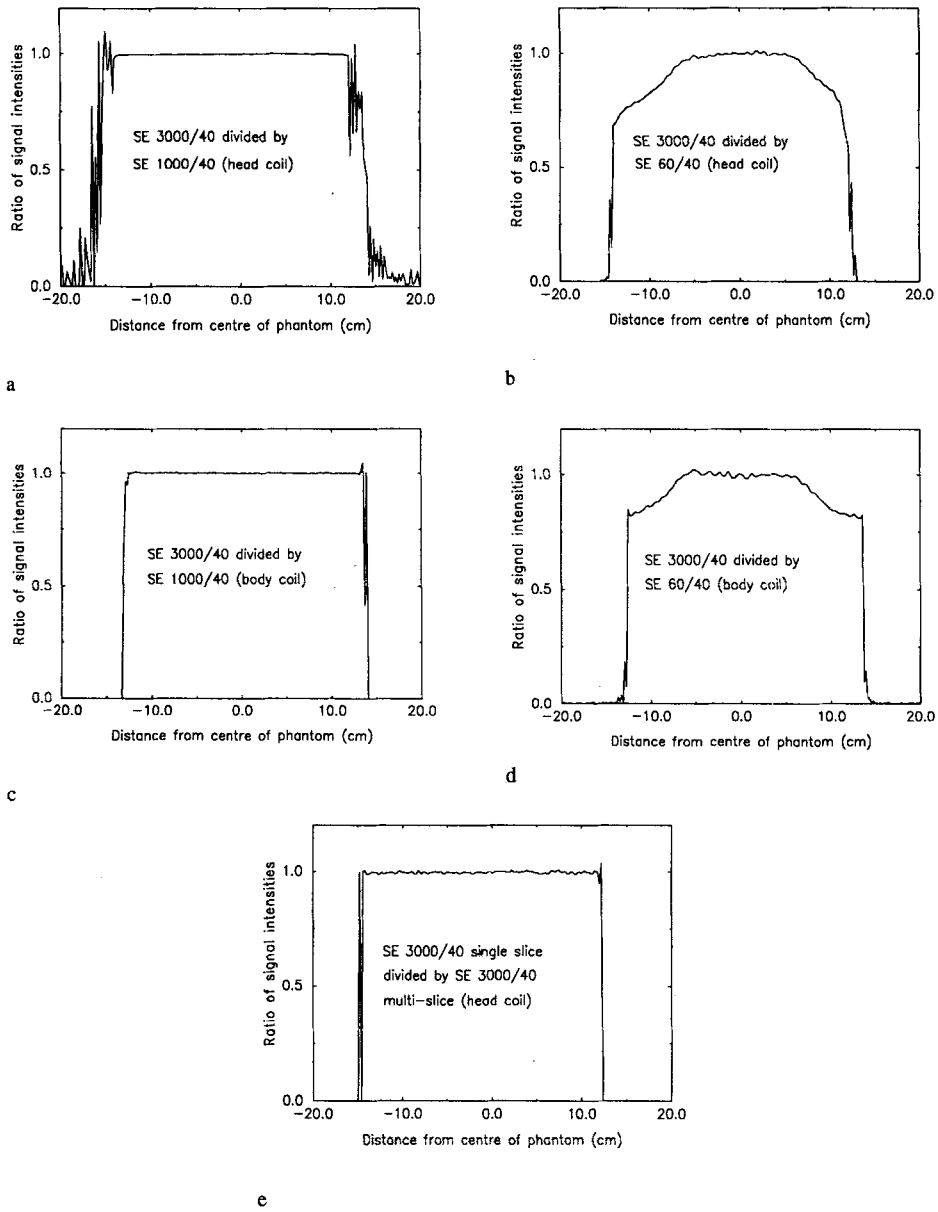

FIG. 4. The effect of varying *TR* on nonuniformity. The figure illustrates axial left/right profiles through a 27.7-cm diameter uniform oil phantom ratio image of (a) SE 3000/40 image divided by an SE 1000/40 image in the head coil, (b) SE 3000/40 image divided by a SE 60/40 image in the head coil. Fifty lines have been averaged to improve SNR. (c) SE 3000/40 image divided by an SE 1000/40 image in the body coil. (d) SE 3000/40 image divided by an SE 60/40 image in the body coil. (e) SE 3000/40 single slice image divided by equivalent slice from SE 3000/40 multislice dataset in the head coil. Each image is normalized to the center of the profile.

differences in echo time, the drop off is not large, but the magnitude increases with increasing difference in echo time. Figure 5b illustrates a profile through a ratio image for the body coil, which demonstrates negligible nonuniformity, suggesting that the effects in the head coil are due to RF nonuniformity, although the mechanism remains unclear.

Variation of Nonuniformity with Number of Echoes

Figure 6 illustrates the difference in nonuniformity between the first, second, and fourth echoes within an echo train. There are relatively large differences between the first and subsequent echoes in a train with subsequent echoes suffering more, presumably as slight inaccuracies in the 180° pulse lead to increasingly poor refocusing. The differences are most apparent in parts of the image further from the coil center, where RF uniformity is poorer.

Difference Between Transverse and Sagittal or Coronal Images

Data acquired at the maximum recommended distance superior to the head coil center with a coronal or sagittal image have a 20–25% greater intensity than equivalent data from axial images. No difference was apparent between sagittal and coronal images. The variation in voxel signal intensity between image orientations is eliminated when GRADWARP is switched off, which strongly implies that there are differences in the manufacturer's method of correction between axial and sagittal or coronal images.

Temporal Stability of Nonuniformity Measurements

Figure 7 illustrates a profile through the least uniform region of each ratio image in the area of the head coil occupied by the head. Each profile is very uniform in

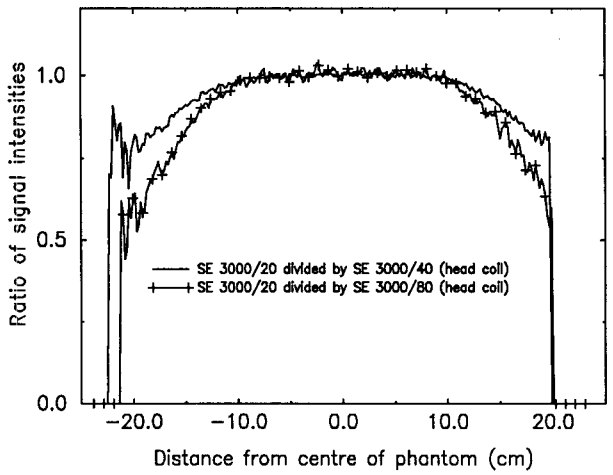

a

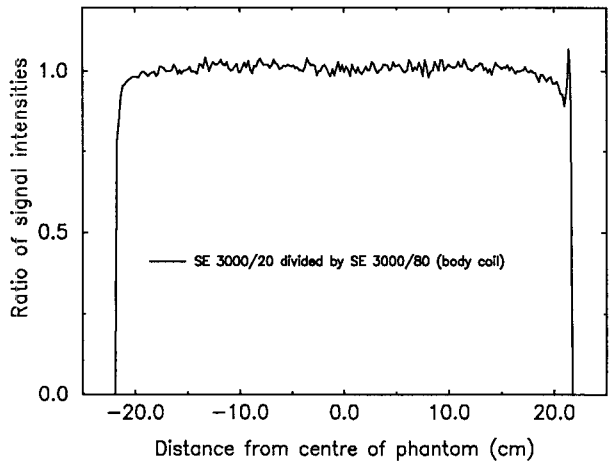

b

FIG. 5. The effect of varying *TE* on nonuniformity. (a) Superior/inferior profile through the ratio of a SE 3000/20 sagittal image divided by a sagittal SE 3000/40 and sagittal SE 3000/80 image for the head coil. The second ratio image has been scaled so the intensity at the center of each ratio image is equal. (b) Superior/inferior profile through the ratio of an SE 3000/20 sagittal image divided by a sagittal SE 3000/80 image for the body coil. The profiles are along the major axis of each coil respectively and have been normalized with respect to the center of the profile.

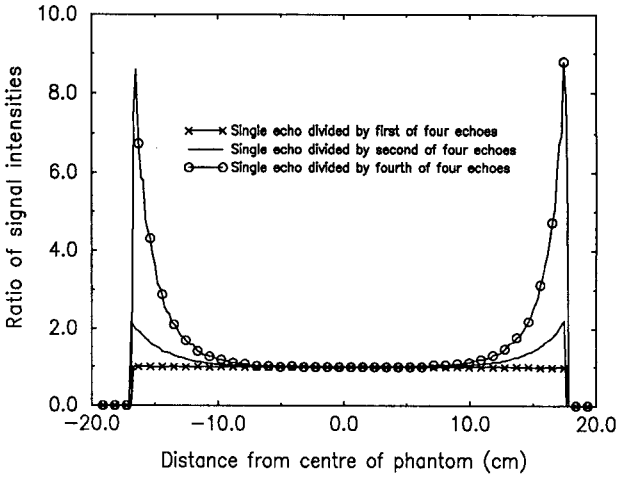

FIG. 6. The effect of echo number on nonuniformity. The figure illustrates superior/inferior profiles through the ratio of (a) an SE 3000/40 sagittal image divided by the first echo of a sagittal SE 3000/40,80,120,160 image acquired using the head coil, (b) a sagittal SE 3000/40 image divided by the second echo from a sagittal SE 3000/20,40,60,80 image acquired using the head coil, and (c) a sagittal SE 3000/80 image divided by the fourth echo from a sagittal SE 3000/20,40,60,80 image acquired using the head coil. Each profile is along the center of the major axis of the head coil and is normalized to its center.

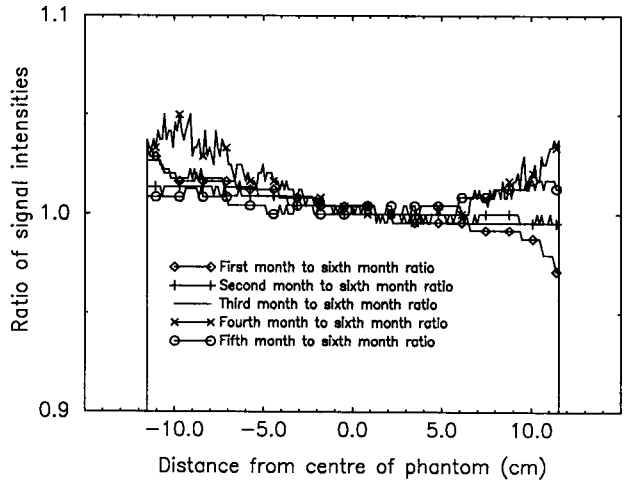

FIG. 7. Anterior/posterior profiles through the most nonuniform region of five ratio datasets created by dividing a reference axial dataset of an oil phantom acquired using the head coil by each of five subsequent datasets acquired over a period of 6 months.

nature; the maximum variation of signal ratio in this region was 4% over the 6-month period. Close to the coil wires and at the end of the coil furthest from the patient, variations in signal ratio could be larger, however, the former possibly due to slight repositioning errors.

Correction of RF Nonuniformity

Figure 8 illustrates the three stages in the method of Lim and Pfefferbaum (a,b,c) and the oil phantom image (d). The maxima and minima in the low pass filtered image may be contrasted with the smoothly varying nonuniformity of the uniform oil phantom. The difference between the two images may be appreciated clearly from horizontal and vertical profiles through the images (e–h). There are several additional disadvantages with the approach of Lim and Pfefferbaum. Firstly, the approach is two-dimensional, so the correct relationship between the intensity of different corrected slices is not guaranteed. A multislice approach using appropriately acquired phantom data without crosstalk does allow a full 3D correction to be made, however (5). Secondly, the method for isolation of the brain only works for nearly axial slices. Thirdly, the approximation that the nonuniformity of a low pass filtered image represents image nonuniformity breaks down when the variation in sensitivity within the field of view is not large relative to the inherent signal

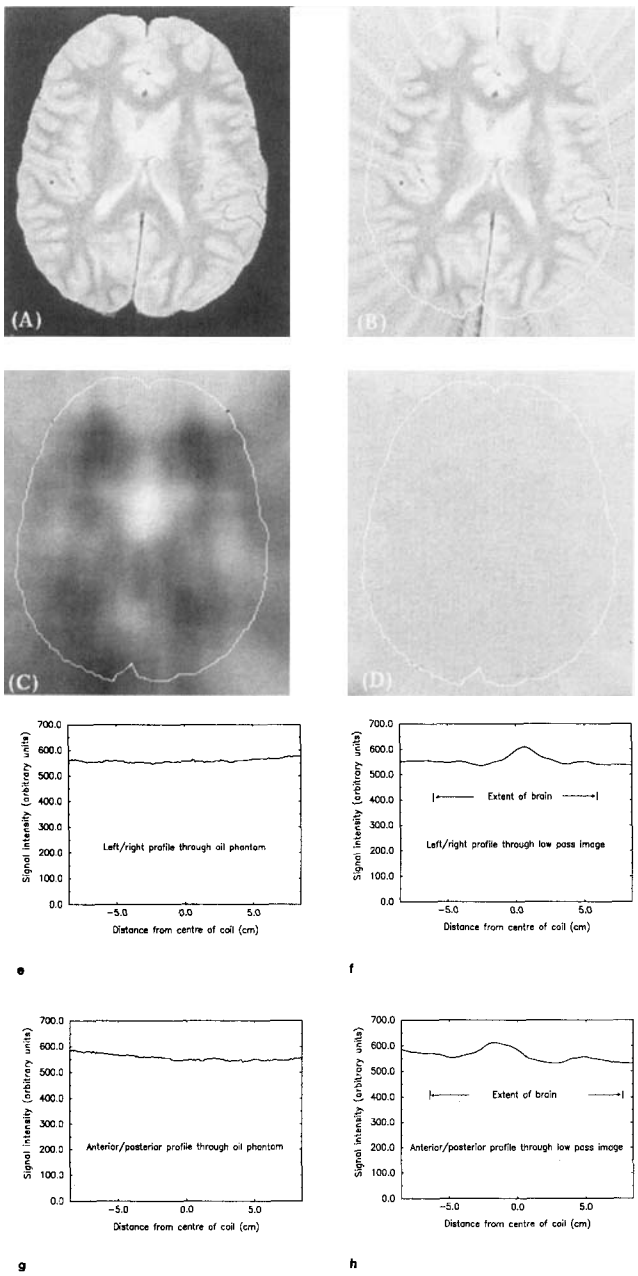

FIG. 8. (a) Skull stripped nearly axial image acquired using the head coil, (b) feathered image, (c) "low pass" version of feathered image. (d) Corresponding image of a uniform oil phantom acquired using the head coil. (e)–(h) illustrate profiles through images (a)–(d).

variation of different tissues. Finally, the low pass filtered image does not accurately reflect image nonuniformity, so the absolute intensity of corrected image pixel values cannot be used for intensity-based processing such as thresholding or clustering.

CONCLUSIONS

Several sources of nonuniformity have been identified here and studied in depth. Although it has been proposed that one set of images for a given pulse sequence could be used to characterize the major image nonuniformities caused by RF transmit and receive inhomogeneities for correction of head coil data (5), we demonstrate that this is not the case for the imager used. Multiecho noncontiguous spin-echo data may, however, be accurately corrected for nonuniformity at longer repetition times using multiecho images of oil phantoms acquired with a *TR* greater than or equal to 1000 ms and approximately the same *TEs*. There are additional effects due to the variation of image nonuniformity with position in a multiecho train and the manufacturer's gradient nonuniformity correction software, however. The latter two effects are often small for standard clinical data acquired using the Signa head coil, but should be considered closely by groups using other imagers. The variation of nonuniformity with *TR*, *TE*, and position in echo train is particularly important for the quantification of T_1 and T_2 as calculation of these values implicitly assume that nonuniformity is equal for all images. It is also important that RF coils are correctly tuned, which for the particular head coil utilized necessitates the use of a "tuning ring" for imaging phantoms. The temporal stability of image nonuniformity as measured using oil phantoms is good for the imager used, and their use for correction of image nonuniformity generally more appropriate than correction based on low pass filtering of images.

REFERENCES

1. A. Simmons, S. R. Arridge, G. J. Barker, P. S. Tofts, Segmentation of neuroanatomy in magnetic resonance images. *Proc. SPIE*, 1652, Newport Beach, California, 2–13 (1992).
2. D. A. G. Wicks, P. S. Tofts, D. H. Miller, G. H. du Boulay, A. Feinstein, R. P. Sacares, I. Harvey, R. Brenner, W. I. McDonald, Volume measurement of multiple sclerosis lesions with magnetic resonance images. *Neuroradiology* **34**, 475–479 (1992).
3. G. J. Barker, P. S. Tofts, Semi-automated quality assurance for quantitative magnetic resonance imaging. *Magn. Reson. Imaging* **10**, 585–596 (1992).
4. B. R. Condon, J. Patterson, D. Wyper, A. Jenkins, D. M. Hadley, Image non-uniformity in magnetic resonance imaging: its magnitude and methods for correction. *Br. J. Radiol.* **60**, 83–87 (1987).
5. D. A. G. Wicks, G. J. Barker, P. S. Tofts, Correction of intensity non-uniformity in MR images of any orientation. *Magn. Reson. Imaging* **11**, 183–196 (1993).
6. A. Simmons, P. S. Tofts, G. J. Barker, D. A. G. Wicks, S. R. Arridge, Considerations for RF nonuniformity correction of spin echo images at 1.5 T, *in* "Proc., SMRM, 11th Annual Meeting, Berlin, 1992," p. 4240.
7. "CRC Handbook of Chemistry and Physics," 69th ed., 1988–89.
8. "UK Medical Devices Directorate," Report MDD/90/44, 1990.
9. R. A. Lerski, D. W. McRobbie, Eurospin II Magnetic Resonance Quality Assessment Test Objects - Instructions for Use, Diagnostic Sonar Ltd, 1992.
10. C. N. Chen, D. I. Hoult, "Biomedical Magnetic Resonance Technology," Adam Hilger, Bristol, UK, 1989.
11. P. A. Bottomley, E. R. Andrew, RF magnetic field penetration, phase shift and power dissipation in biological tissue: implications for NMR imaging. *Phys. Med. Biol.* **23**, 630–643, 1978.
12. P. S. Tofts, G. J. Barker, D. A. G. Wicks, D. MacManus, A. Simmons, D. H. Miller, Correction of non-uniform sensitivity in multi-array surface coil images of the spinal cord, and

reformatting that preserves on film their spatial resolution, *in* "Proc., SMRM, 11th Annual Meeting, Berlin, 1992," p. 4241.
13. P. J. Nummi, E. K. Luoma, R. K. Raininko, J. A. Pohjonen, Direct phantom intensity correction in imaging of the spine, *in* "Proc., SMRM, 11th Annual Meeting, Berlin, 1992," p. 4251.
14. E. R. McVeigh, M. J. Bronskill, R. M. Henkelman, Phase and sensitivity of receiver coils in magnetic resonance imaging. *Med. Phys.* **13,** 806–814 (1986).
15. S. J. Nelson, D. B. Vigneron, J. Kurhanewicz, H. Sakuma, S. Moyher, D. A. C. Kelley, Correction of MR images for the reception profile of surface and endorectal coils, *in* "Proc., SMRM, 11th Annual Meeting, Berlin, 1992," p. 4252.
16. R. B. Lufkin, T. Sharpless, B. Flannigan, W. Harafee, Dynamic-range compression in surface-coil MRI. *Am. J. Roentgen.* **147,** 379–382 (1986).
17. J. Haslegrove, M. Prammer, An algorithm for compensation of surface coil images for sensitivity of the surface coil. *Magn. Reson. Imaging* **4,** 469–472 (1986).
18. M. Fuderer, A. van Est, Surface coil intensity correction using homomorphic filtering, *in* "Proc., SMRM, 6th Annual Meeting, New York, 1987," p. 266.
19. L. Axel, J. Costantini, J. Listerud, Intensity correction in surface-coil imaging. *Am. J. Roentgen.* **148,** 418–420 (1987).
20. K. O. Lim, A. Pfefferbaum, Segmentation of MR brain images into cerebrospinal fluid spaces, white and grey matter. *J. Comput. Assist. Tomogr.* **13,** 588–593 (1989).
21. R. A. Lerski, D. W. McRobbie, K. Straughan, P. M. Walker, J. D. de Certaines, A. M. Bernard, Multi-center trial with protocols and prototype test objects for the assessment of MRI equipment. *Magn. Reson. Imaging,* **6,** 201–214 (1988).
22. B. I. Bleaney, B. Bleaney, "Electricity and Magnetism," 3rd ed., Oxford Science Publications, 1976.
23. "Signa Users Manual," General Electric, Milwaukee, WI.
24. G. Johnson, I. E. G. Ormerod, D. Barnes, P. S. Tofts, D. MacManus, Accuracy and precision in the measurement of relaxation times from nuclear magnetic resonance images. *Br. J. Radiol.* **60,** 143–153 (1987).
25. J. B. Kneeland, A. Shimakawa, F. W. Wehrli, Effect of intersection spacing on MR image contrast and study time. *Radiology* **158,** 819–822 (1986).
26. A. Simmons, G. J. Barker, P. S. Tofts, S. R. Arridge, Quantitation of Geometric Distortions at 1.5 T, *in* "Proc., SMRM, 12th Annual Meeting, New York, 1993," p. 747.
27. C. E. Hayes, W. A. Edelstein, J. F. Schenck, O. M. Mueller, M. Eash, An efficient, highly homogeneous radiofrequency coil for whole-body NMR imaging at 1.5 T. *J. Magn. Reson.* **63,** 622–628 (1985).
28. G. H. Glover, S. Connolly, A. Shimakawa, Variable rate selective RF pulses for time reversal and saturation, *in* "Proc., SMRM, 6th Annual Meeting, New York, 1987," p. 159.